

Microstructure, phase structure and electrical properties of $0.954\text{K}_{1-x}\text{Na}_x\text{NbO}_3-0.04\text{Bi}_{0.5}\text{Na}_{0.5}\text{ZrO}_3-0.006\text{BiFeO}_3$ lead-free ceramics

Jian Ma² · Bo Wu¹ · Wenjuan Wu¹ · Min Chen¹

Received: 9 October 2016 / Accepted: 11 November 2016 / Published online: 14 November 2016
© Springer Science+Business Media New York 2016

Abstract In this work, $0.954\text{K}_{1-x}\text{Na}_x\text{NbO}_3-0.04\text{Bi}_{0.5}\text{Na}_{0.5}\text{ZrO}_3-0.006\text{BiFeO}_3$ ($\text{KN}_x\text{N}-\text{BNZ}-\text{BF}$) lead-free ceramics were fabricated by conventional ceramic technique. The effect of K/Na ratio on microstructure, phase structure and electrical properties was systematically investigated. The orthorhombic-tetragonal phase transition temperature ($T_{\text{O-T}}$) increases and rhombohedral-orthorhombic phase transition temperature ($T_{\text{R-O}}$) drops simultaneously with increasing the Na content, leading to an R-O-T phase boundaries in the ceramics with $0.44 \leq x \leq 0.60$. By tailoring their K/Na ratio and optimizing the sintering temperature, an enhanced electrical properties (e.g. $d_{33} \sim 438$ pC/N, $k_p \sim 0.51$, $T_c \sim 320$ °C, $\epsilon_r \sim 2304$ and $\tan \delta \sim 0.029$) was obtained at the ceramics with $x = 0.56$ sintered at 1090 °C, which could be attributed to the preferably density as well as the R-O-T phase boundary nearer the room temperature. Therefore, we think that the $\text{KN}_x\text{N}-\text{BNZ}-\text{BF}$ ceramic is a promising candidate for piezoelectric devices.

1 Introduction

Due to the sustainable development and the governmental regulations against hazardous substances, lead-free piezoelectric ceramics have become a hotspot of the current

researches to substitute for lead zirconate titanate (PZT) ceramics which contain a large amount of toxic Pb [1–4]. Recently, several promising candidates have been given much efforts to the development of competitive lead-free counterparts, such as $\text{Bi}_{1/2}\text{Na}_{1/2}\text{TiO}_3$ -based (BNT), BaTiO_3 -based (BT) and (K, Na) NbO_3 -based (KNN) ceramics [5–18].

As we known, among those lead-free perovskite-based piezoelectric ceramics, (K, Na) NbO_3 -based piezoelectric ceramics have been mainly focused because of the high Curie temperature (T_c) and relatively large piezoelectric properties [12–18]. To improve the properties of KNN ceramics, composition optimization has been regarded as an effective way to achieve this objective [19, 20]. For example, refining the K/Na ratio, adding ABO_3 additives, adjusting the amount of Sb or Ta elements [21–27]. According to the phase diagram of $\text{K}_{1-x}\text{Na}_x\text{NbO}_3$ solid solutions, we can find that the $\text{KNbO}_3/\text{NaNbO}_3$ (K/Na) have strongly effect on the phase structure, for example, an orthorhombic phase structure (O) is observed at $x = 0$ and 1, and a series of separate phase boundaries at the room temperature are identified at $x = 0.525$, 0.675 and 0.825 [28, 29]. In addition, researchers found that the K/Na ratio could also strongly affect the microstructure and electrical properties of KNN-based ceramics [24–27]. Therefore, an enhanced property of KNN-based ceramics may be obtained by refining the K/Na ratio.

It is reported that a large d_{33} is normally obtained by sacrificing its T_c in KNN-based material system, which seriously hinder their practical applications [7]. Recently, a material system of $(1-x-y)\text{K}_{0.48}\text{Na}_{0.52}\text{NbO}_3-y\text{Bi}_{0.5}\text{Na}_{0.5}\text{ZrO}_3-x\text{BiFeO}_3$ with large d_{33} and high T_c was designed to solve contradict of d_{33} and T_c each other by optimizing the composition of $\text{Bi}_{0.5}\text{Na}_{0.5}\text{ZrO}_3$ and BiFeO_3 which can shift the $T_{\text{R-O}}$ and $T_{\text{O-T}}$ simultaneously to the room temperature [9, 11, 19]. However, the d_{33} is not comparable to the high

✉ Bo Wu
wubo7788@126.com

¹ Sichuan Province Key Laboratory of Information Materials and Devices Application, Chengdu University of Information Technology, Chengdu 610225, People's Republic of China

² Physics Department, Southwest University for Nationalities, Chengdu 610041, People's Republic of China

performance of PZT-based ceramics (e.g. PZT-5H, PZT-5J, PZT-5R) [35]. To further enhance the properties of this material system, the $0.954\text{K}_{1-x}\text{Na}_x\text{NbO}_3-0.04\text{Bi}_{0.5}\text{Na}_{0.5}\text{ZrO}_3-0.006\text{BiFeO}_3$ ($\text{KN}_x\text{N-BNZ-BF}$, $0.44 \leq x \leq 0.68$) lead-free ceramics was designed by tailoring their K/Na ratio. The effect of K/Na ratio on the microstructure, phase structure and electrical properties of the ceramics are systematically investigated. In addition, it is reported that the sintering parameters, especially the sintering temperature, are the key factors to determine the piezoelectric properties of lead-free ceramics [10, 30, 31]. In this work, the relationship of sintering temperature, density and piezoelectric properties are investigated in detail. By tailoring their K/Na ratio and optimizing the sintering temperature, an optimal electrical properties was obtained in the ceramics with $x = 0.56$ sintered at 1090°C , and the related underlying physical mechanisms for the properties are discussed.

2 Experimental procedure

$0.954\text{K}_{1-x}\text{Na}_x\text{NbO}_3-0.04\text{Bi}_{0.5}\text{Na}_{0.5}\text{ZrO}_3-0.006\text{BiFeO}_3$ ($0.44 \leq x \leq 0.68$) piezoelectric ceramics were prepared by the conventional solid-state reaction process. Na_2CO_3 (99.8%), K_2CO_3 (99%), Bi_2O_3 (99%), Nb_2O_5 (99.5%), Fe_2O_3 (99%), and ZrO_2 (99%) were used as raw materials. All raw materials of this work were produced by Sinopharm Chemical Reagent Co., Ltd. Raw materials were weighed according to the designed chemical formula, and milled with ZrO_2 balls for 24 h with alcohol as the dispersion medium, and then dried and calcined at 850°C for 6 h in air. These calcined powders were mixed with a binder of 8 wt% polyvinyl alcohol (PVA) and pressed into the pellets with 10 mm diameter and 1 mm thickness under a pressure of 10 MPa. The PVA was burnt off afterwards. All disk samples were sintered at $1080-1100^\circ\text{C}$ for 3 h in air after the PVA binder was burnt out. All the samples were polarized in

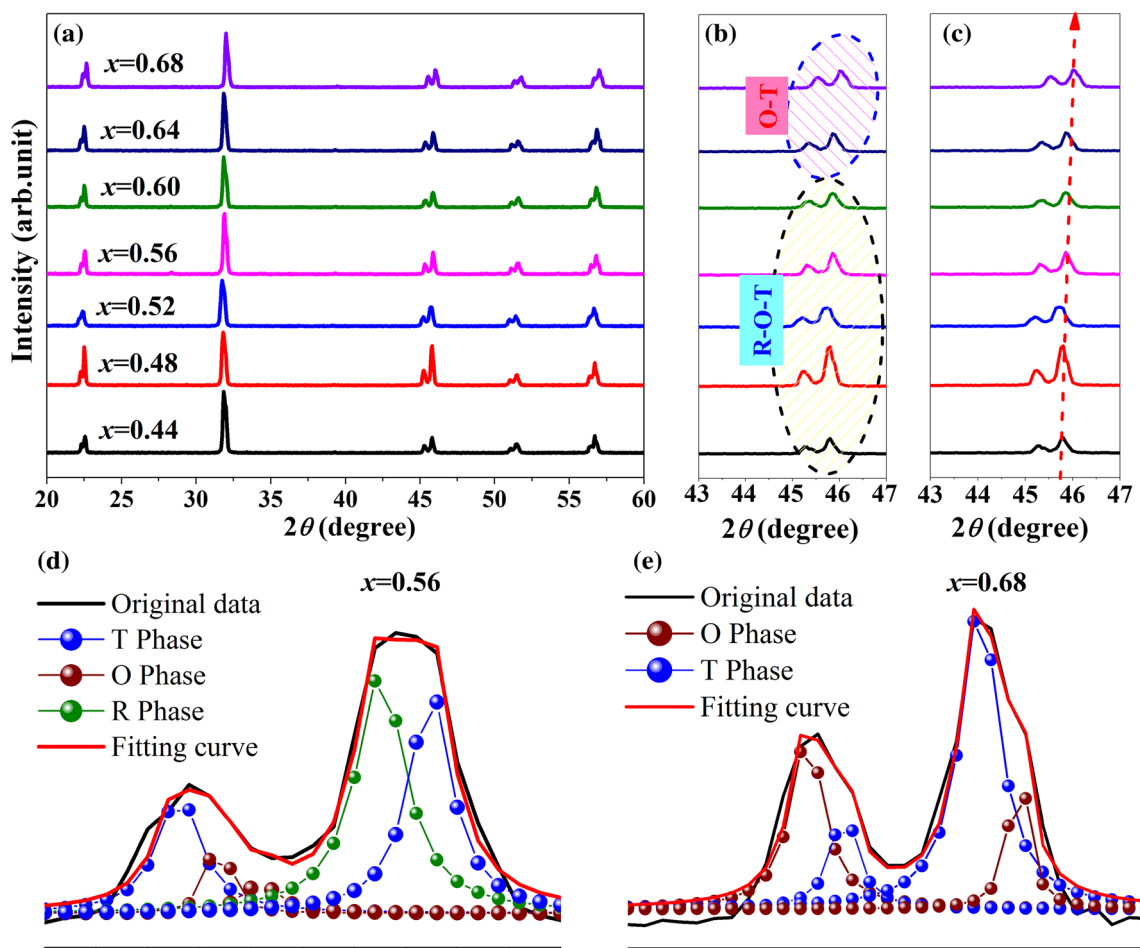


Fig. 1 XRD patterns of the $\text{KN}_x\text{N-BNZ-BF}$ ceramics in the 2 theta range of **a** $20^\circ-60^\circ$, **b**, **c** $43^\circ-47^\circ$, and **d**, **e** XRD patterns simulated by the Lorentz method of the ceramics with $x = 0.56$ and 0.68 , respectively

a silicone oil bath at 20 °C under a *dc* field of 3.0–4.0 kV/mm for 15 min.

X-ray diffraction meter with a CuK α radiation (DX-2700, Dandong, China) has been used to identify the phase structure of the sintered cylindrical pellets. Their microstructure and chemical compositions were measured by a field-emission scanning electron microscope (FE-SEM) (JSM-7500, Japan). The density of the ceramics was measured by the Archimedes method. The capacitance and dissipation factors of the sintered samples were measured using an LCR analyzer (HP 4980, Agilent, U.S.A.) with varied temperatures between –150 and 200 °C and room temperature \sim 550 °C. The polarization versus electric field (*P*–*E*) hysteresis loops of the unpoled cylindrical pellets were measured at 10 Hz with a ferroelectric tester (Radiant Technologies, Inc. Albuquerque, NM, USA). Their planar electromechanical coupling factor (k_p) was measured by a resonance–antiresonance method with an impedance analyzer (Impedance Analyzer, PV70A, Beijing, China). The d_{33} was measured with a commercial

Berlincourt-type d_{33} m (ZJ-3A, China) for the poled samples.

3 Results and discussion

Figure 1a plots the room temperature XRD patterns of the KN $_x$ N–BNZ–BF ceramics as a function of x . All samples display a pure perovskite structure without the occurrence of secondary phases, indicating that a homogeneous solid solution can be formed in the studied range of K/Na ratio. Figure 1b shows the corresponding expanded XRD patterns of KN $_x$ N–BNZ–BF ceramics, measured at $2\theta = 43^\circ$ – 47° . One can find that the mixed phases appear in all ceramics, and the specific phase compositions of each sample needs to be further confirmed by their corresponding ϵ_r –*T* curves (–150 to 200 °C). As shown from Fig. 2a–c, the orthorhombic–tetragonal phase transition temperature (T_{O-T}) and rhombohedral–orthorhombic phase transition temperature (T_{R-O}) of the ceramics are very

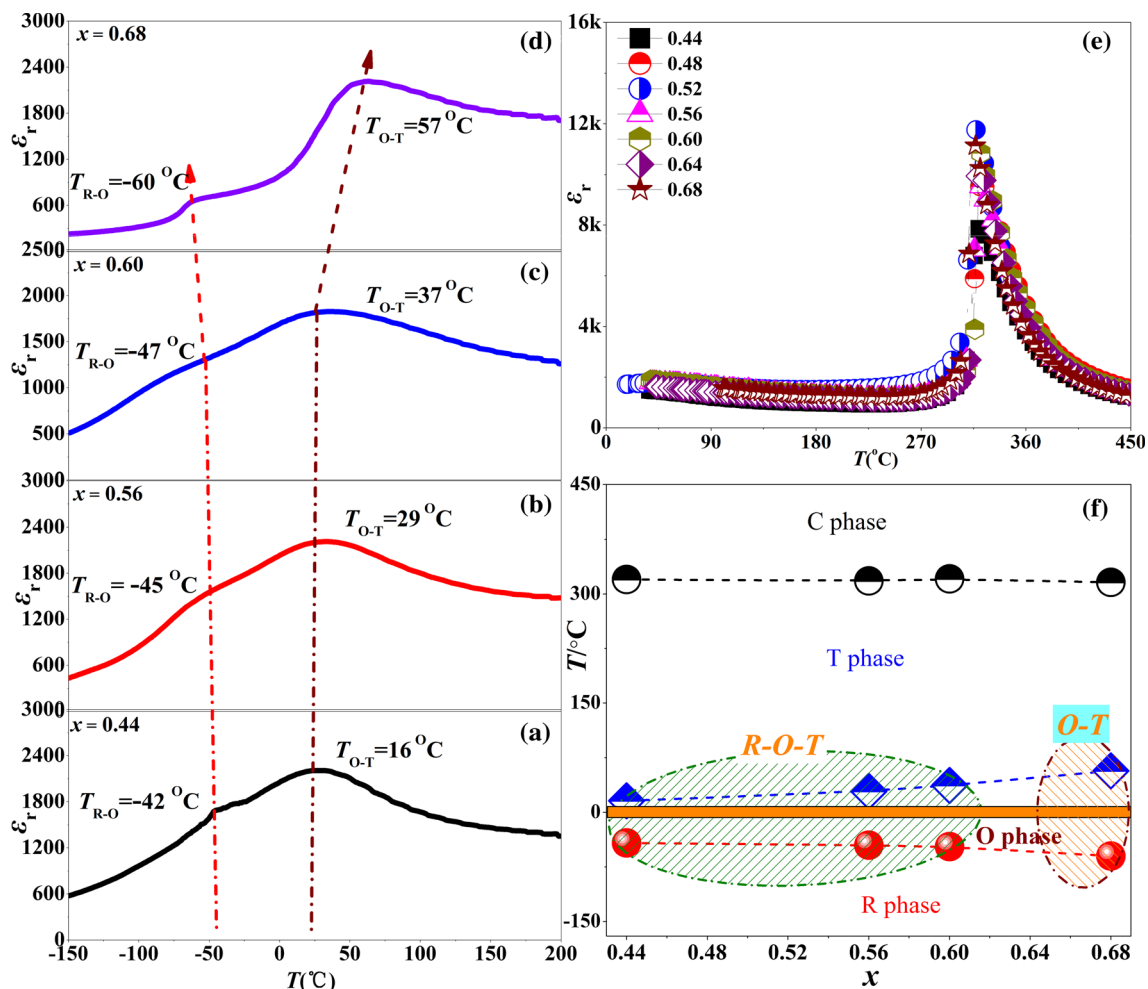


Fig. 2 ϵ_r –*T* curves of KN $_x$ N–BNZ–BF ceramics of **a–d** –150 to 200 °C, **e** 20–450 °C, and **f** Phase diagrams of KN $_x$ N–BNZ–BF ceramics

sensitive to the K/Na ratio, that is, the T_{O-T} ($16 \rightarrow 37 \text{ }^\circ\text{C}$) increases and T_{R-O} ($-42 \rightarrow -47 \text{ }^\circ\text{C}$) decreases with increasing the Na content from 0.44 to 0.60. Considering the T_{O-T} and T_{R-O} of the ceramics ($x = 0.44-0.60$) are close to room temperature, an R–O–T phase boundary is identified in this compositions. Continuing increasing the Na content, the T_{O-T} ($37 \rightarrow 57 \text{ }^\circ\text{C}$) and T_{R-O} ($-47 \rightarrow -60 \text{ }^\circ\text{C}$) are simultaneously away from room temperature, indicating that an O–T phase boundary is formed in the ceramics with $0.60 < x \leq 0.68$. To further clarify their phase structure, the simulated XRD patterns of $x = 0.56$ and 0.68 were carried out by the Lorentz method, as is shown in Fig. 1d, e. One can find that the experimental XRD patterns of the samples can be regarded as the mixture of the several separated peaks, corresponding to the characteristic diffraction peaks of R, O, or T phases, that is, the ceramics with $x = 0.56$ and 0.68 possess the R–O–T and O–T multiphase coexistence, respectively. In

addition, the XRD peaks of $\text{KN}_x\text{N–BNZ–BF}$ ceramics shift to a high angle with increasing Na content, as is shown in Fig. 1c. Undoubtedly, the shift of diffractions can be attributed to the different ionic diameter of K^+ (1.33 \AA) and Na^+ (0.97 \AA), that is, the lattice constant of $\text{KN}_x\text{N–BNZ–BF}$ ceramics decreases by Na^+ substitution of a part of K^+ , leading to the shifting of XRD peaks to high angle. As a result, an R–O–T phase boundary has been identified in the ceramics of $0.044 \leq x \leq 0.60$.

Figure 2e plots the temperature dependence of dielectric constant (ϵ_r-T) curves ($20-450 \text{ }^\circ\text{C}$) of the $\text{KN}_x\text{N–BNZ–BF}$ ceramics. All ceramics present one phase transition temperature, corresponding to tetragonal-cubic phase transition temperature (T_C) at high temperature. Figure 2f addresses the phase diagrams of $\text{KN}_x\text{N–BNZ–BF}$ ceramics. We can find that K/Na ratio has different effects on their phase transition temperature (T_{O-T} , T_{R-O} and T_C). With the increase of Na content, the T_{R-O} and T_{O-T} are

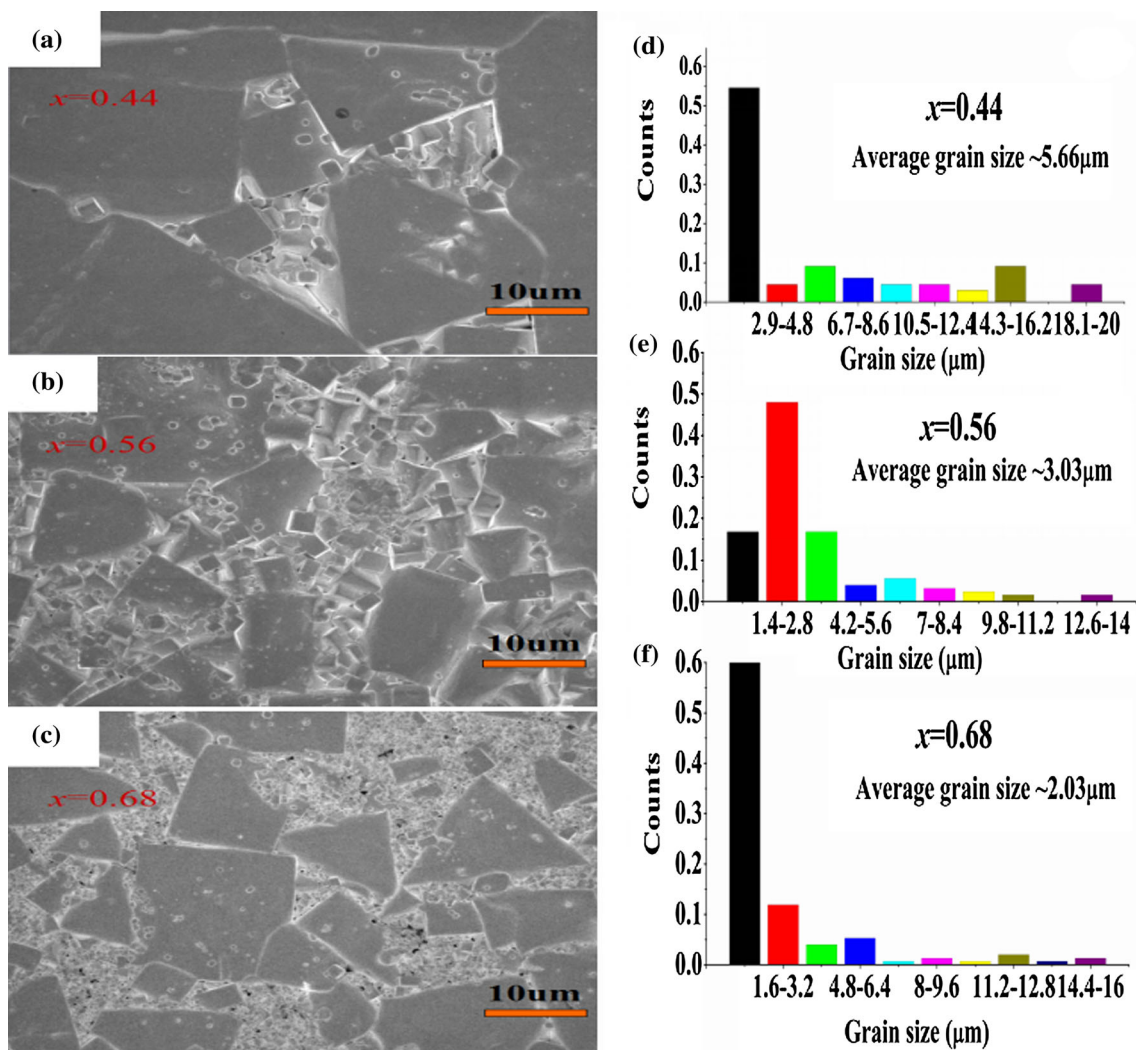


Fig. 3 a–c SEM surface images and d–f grain size distribution of $\text{KN}_x\text{N–BNZ–BF}$ ceramics

simultaneously away from room temperature and T_C (~ 320 °C) almost remain unchanged.

Figure 3 shows the SEM surface morphologies and the grain size distributions of $\text{KN}_x\text{N-BNZ-BF}$ ceramics sintering at 1090 °C. All ceramics present a bimodal grain size distribution, and small grains are located at the gaps of large ones, leading to a dense microstructure except the ceramics with $x = 0.68$ (some pores was observed in this composition), which is important for the enhanced electrical properties [19]. In addition, one can see that the grain size ($\sim 5.66 \rightarrow 2.03$ μm) gradually decreases with increasing Na content, suggesting that the grain size is very sensitive to the K/Na ratio, a similar phenomenon was observed in others research [24–27, 32]. It can be explained

that the melting point of Na is higher than K, and then the growth of grains is inhibited by increasing Na content, resulting in a smaller grain in the ceramics of high Na content [2, 32, 33]. As a result, the decrease in grains of all ceramics should be attributed to the increasing Na content.

To identify the composition difference of the cross section, the EDS spectrum of the cross morphologies for $\text{KN}_x\text{N-BNZ-BF}$ ceramics were carried out, as is shown in Fig. 4. One can find that the results well match to the experimental purpose as designed. In other words, the peak intensity that the Na content increases and the K content drops, as shown in Fig. 4d–f. Figure 5 plots the change of theoretical and experimental K/Na values of $\text{KN}_x\text{N-BNZ-BF}$ ceramics. We can find that theoretic value of the cross

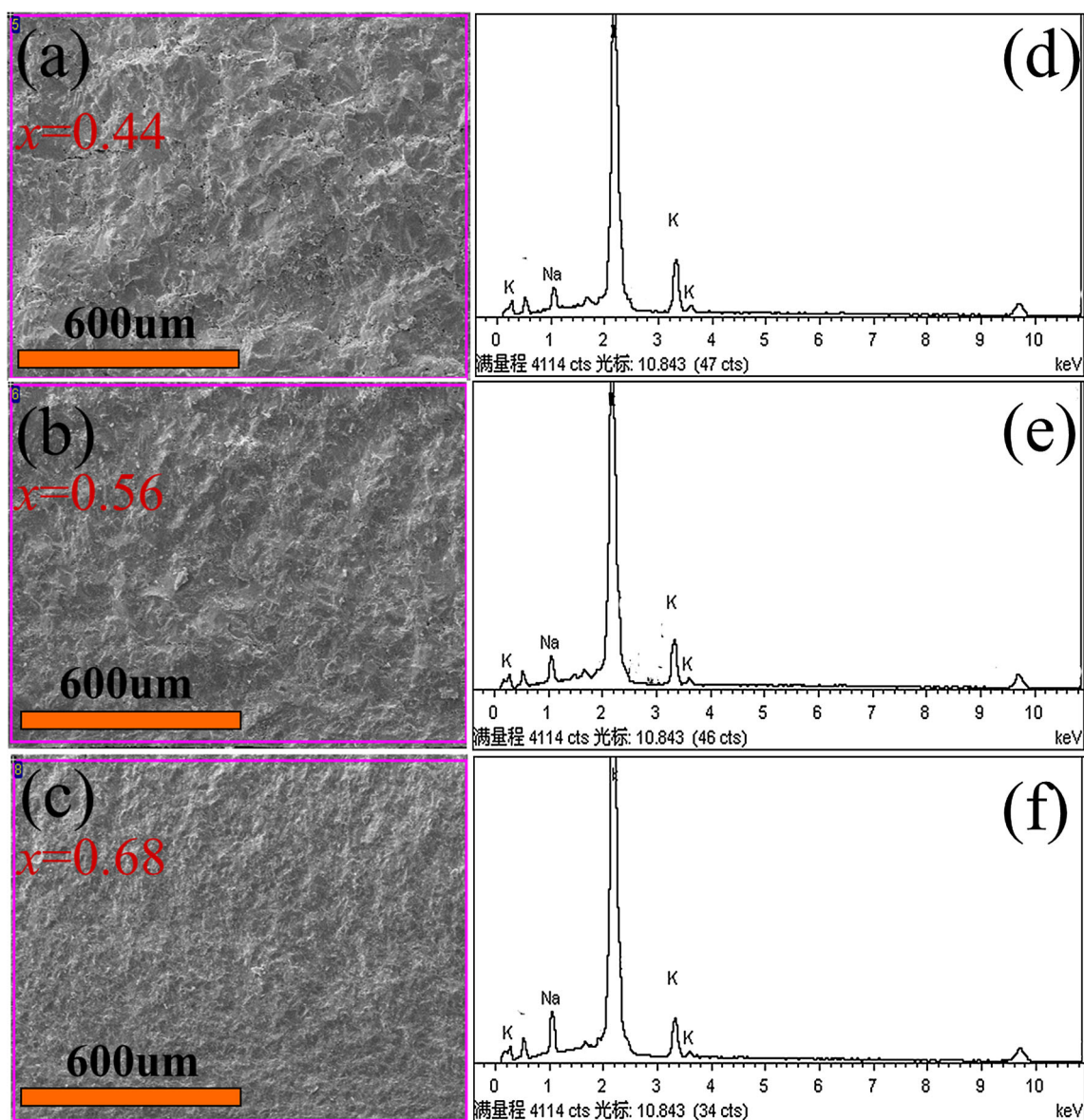


Fig. 4 Composition analysis of K/Na of cross section of $\text{KN}_x\text{N-BNZ-BF}$ ceramics

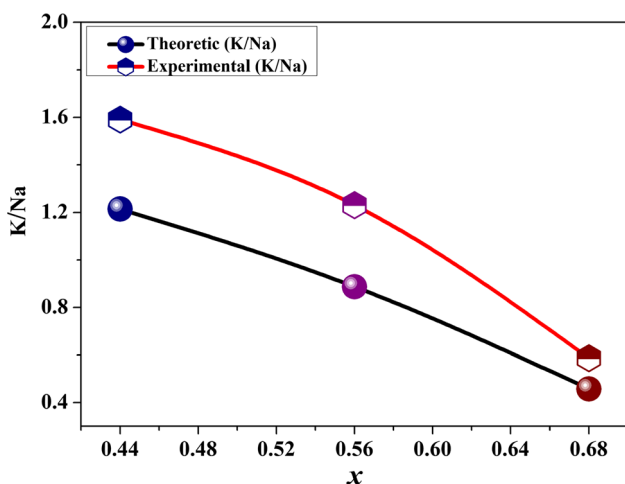


Fig. 5 Theoretic and experimental of K/Na values in $\text{KN}_x\text{N-BNZ-BF}$ ceramics

section is slightly lower than that of the experimental K/Na value of the ceramics. Moreover, the experimental and theoretical of K/Na values of this ceramics exhibit a similar variation trend, indicating that experimental and theoretical results of K/Na ratio almost keep consistent. Therefore, the results of the cross section almost illustrate the intrinsic characteristics of materials.

Figure 6a shows the P - E loops of $\text{KN}_x\text{N-BNZ-BF}$ ceramics. All ceramics present saturated ferroelectric P - E loops, indicating that the $\text{KN}_x\text{N-BNZ-BF}$ ceramics have a typical ferroelectricity [34]. Figure 6b plots the P_r and E_c of $\text{KN}_x\text{N-BNZ-BF}$ ceramics. P_r of the ceramics slightly fluctuates in the range of 18.5–25.2 $\mu\text{C}/\text{cm}^2$ because of the multiphase coexistence. In addition, E_c of the ceramics first drops and then increases, getting a lower E_c (~ 10.1 kV/cm) at $x = 0.56$. As a result, the enhanced ferroelectric behavior could be attributed to the coexistent phase boundary region (R-O-T or O-T).

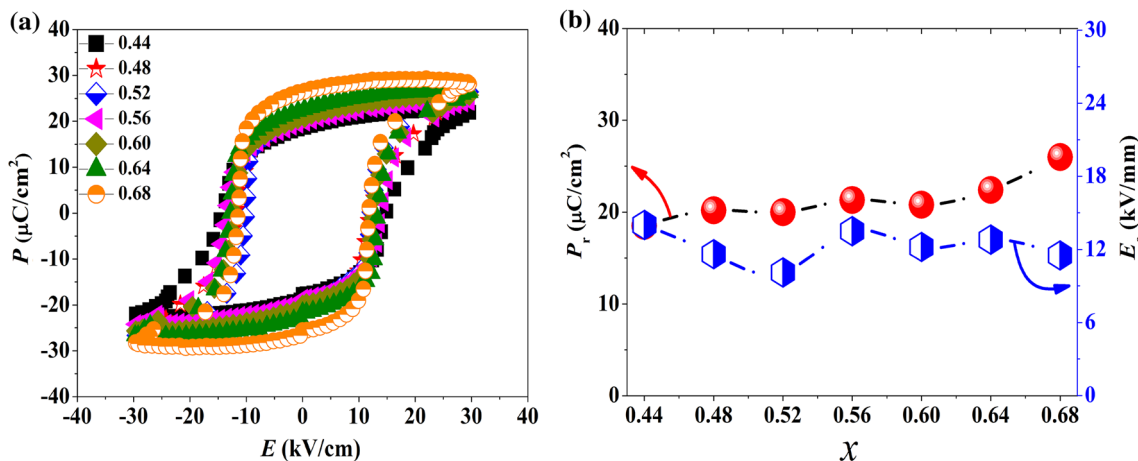


Fig. 6 a P - E loops and b P_r and E_c of $\text{KN}_x\text{N-BNZ-BF}$ ceramics

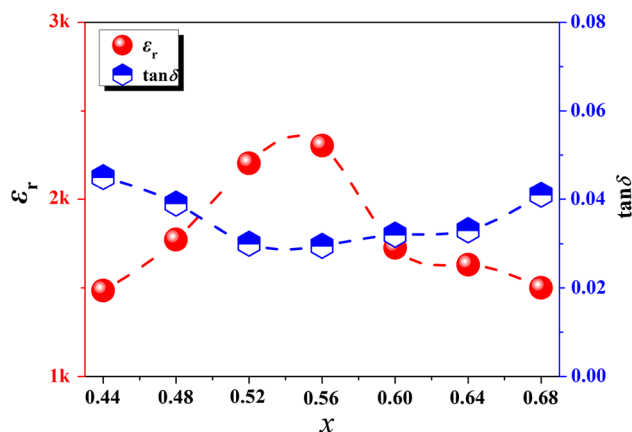


Fig. 7 ϵ_r and $\tan \delta$ of $\text{KN}_x\text{N-BNZ-BF}$ ceramics

Figure 7 plots the room temperature ϵ_r and $\tan \delta$ values of $\text{KN}_x\text{N-BNZ-BF}$ ceramics, measured at 100 kHz. Obviously, the ϵ_r value of $\text{KN}_x\text{N-BNZ-BF}$ ceramics increases in the compositional range of 0.44–0.56, and then decrease with further increasing Na content (0.60–0.68) due to the lower density as well as the formation of some pores (see Figs. 3c, 8b), getting an optimal value of 2304 at $x = 0.56$. The $\tan \delta$ values of $\text{KN}_x\text{N-BNZ-BF}$ ceramics decreases in the range of 0.44–0.56, and then increases with increasing Na content (0.56–0.68), a lower $\tan \delta$ (~ 0.029) was obtained at $x = 0.56$. Therefore, an optimal dielectric properties ($\epsilon_r \sim 2304$, $\tan \delta \sim 0.029$) was obtained at $x = 0.56$ because of the coexistent phase boundary (R-O-T) and preferably density.

Figure 8a plots the composition dependence of piezoelectric properties (d_{33} , k_p and Q_m) in the ceramics, measured at room temperature. We can see that piezoelectric properties (d_{33} , k_p and Q_m) are strongly dependent on the Na content, that is, an appropriate amount of Na content could promote the piezoelectric properties, while the excess Na lead to an adverse consequence. With increasing the Na content, the d_{33}

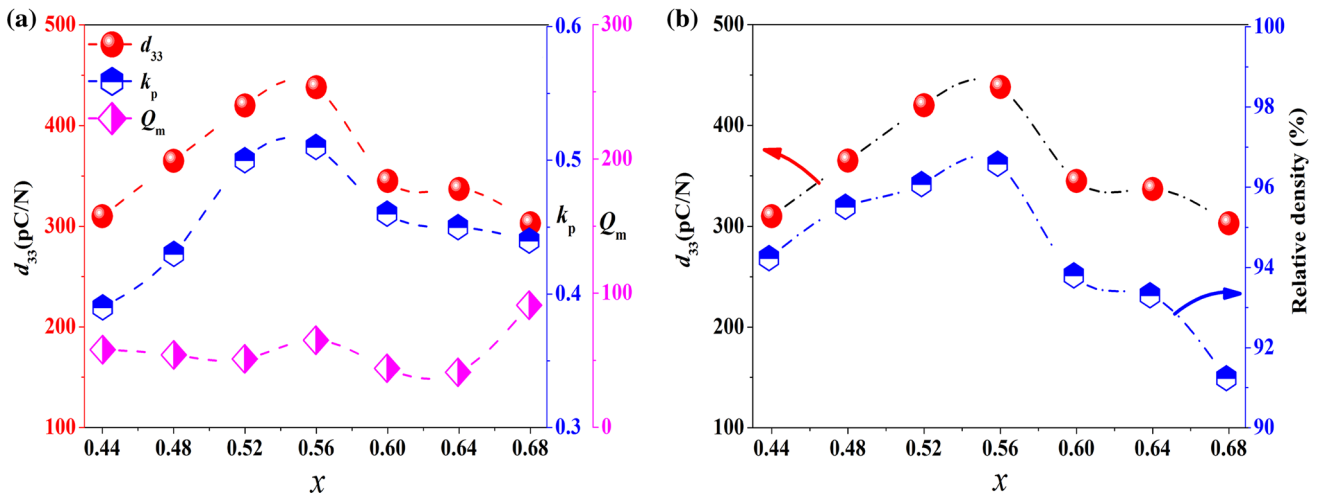


Fig. 8 a piezoelectric properties (d_{33} , k_p and Q_m) of $\text{KN}_x\text{N-BNZ-BF}$ ceramics; and b d_{33} and relative density of $\text{KN}_x\text{N-BNZ-BF}$ ceramics

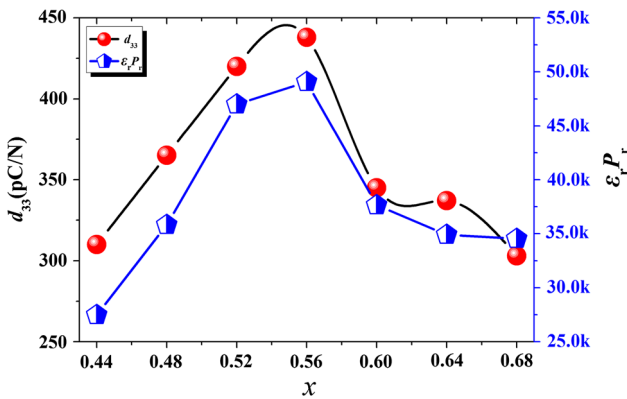


Fig. 9 d_{33} and $\epsilon_r P_r$ of $\text{KN}_x\text{N-BNZ-BF}$ ceramics

and k_p values increase first and then drop, an optimal piezoelectric behaviors ($d_{33} \sim 438$ pC/N, $k_p \sim 0.51$) of $\text{KN}_x\text{N-BNZ-BF}$ ceramics was obtained at $x = 0.56$ because of the R–O–T phase boundary nearer the room temperature. It can be explained that the R–O–T phase boundary near room temperature of $x = 0.56$ can provide more possibilities of polarization orientations and rotation of ferroelectric domains, enhancing the piezoelectric properties of the ceramics [11]. In addition, the Q_m value of $\text{KN}_x\text{N-BNZ-BF}$ ceramics fluctuates in the range of 44–91. Figure 8b plots the d_{33} and relative density of $\text{KN}_x\text{N-BNZ-BF}$ ceramics. The d_{33} value and relative density of $\text{KN}_x\text{N-BNZ-BF}$ ceramics exhibit a similar variation trend, and a higher relative density ($\sim 96.5\%$) was obtained at $x = 0.56$, indicating that a better

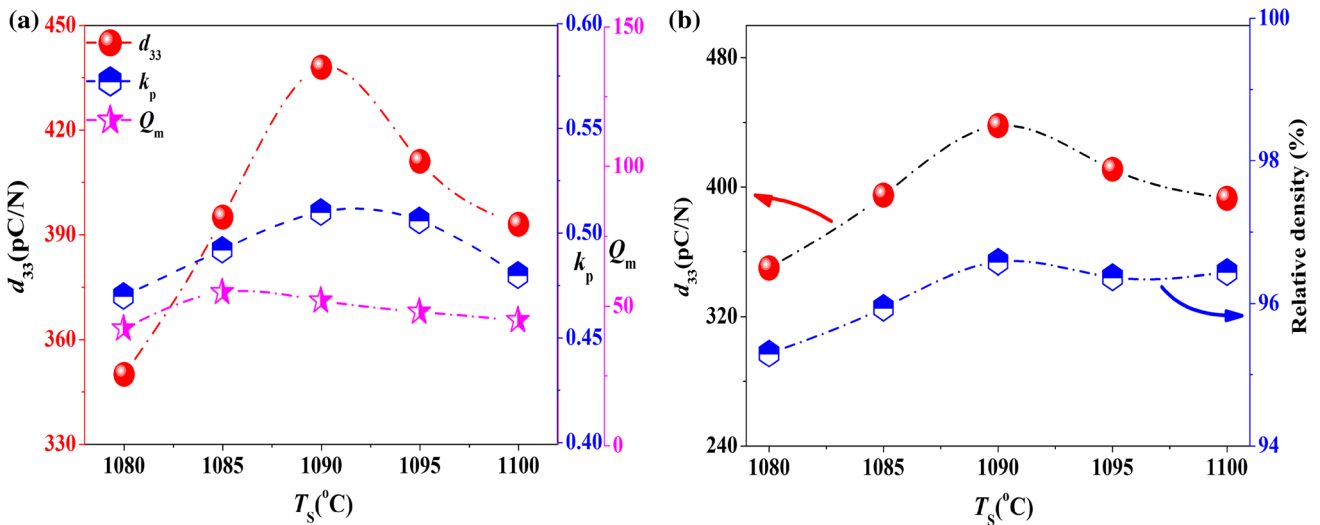


Fig. 10 a piezoelectric properties (d_{33} , k_p and Q_m) and b d_{33} and relative density of $\text{KN}_{0.56}\text{N-BNZ-BF}$ ceramics as a function of sintering temperature

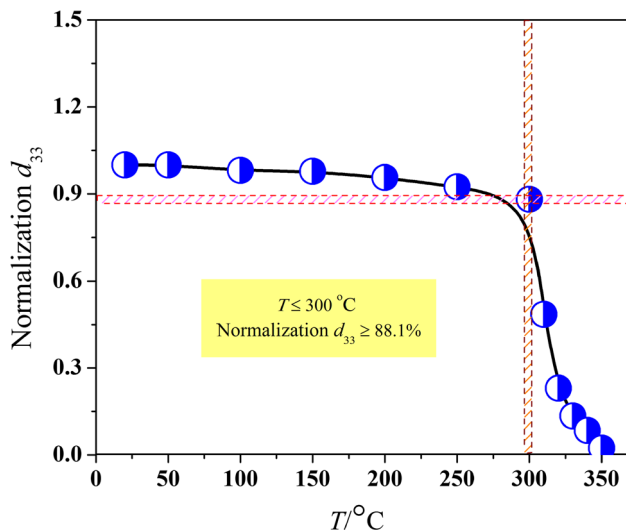


Fig. 11 Normalization d_{33} versus annealing temperature of $\text{KN}_{0.56}\text{N-BNZ-BF}$ ceramics

density microstructure can promote the piezoelectricity. To further illuminate the underlying physical mechanism, the curves of both d_{33} and $\varepsilon_r P_r$ versus x was carried out in Fig. 9. Both the maximum d_{33} and the maximum $\varepsilon_r P_r$ could be achieved in the ceramics of $x = 0.56$, confirming that the enhanced piezoelectricity could be attributed to the enhanced dielectric and ferroelectric properties [11, 19, 20]. As a result, the R–O–T phase boundary, preferably density as well as the enhanced dielectric and ferroelectric properties can promote the piezoelectric properties.

It is reported that the sintering temperature is the crucial factor to determine the piezoelectric properties of lead-free ceramics [10, 30, 31]. In this work, a curve of the piezoelectric properties (d_{33} , k_p and Q_m) of $\text{KN}_{0.56}\text{N-BNZ-BF}$ ceramics versus sintering temperature was carried out, as is shown in Fig. 10a. With increasing the sintering temperature from 1080 to 1090 °C, the d_{33} value of the ceramics sharply increases, and then drops with a further increase of sintering temperature to 1110 °C, reaches a maximum value of $d_{33} \sim 438$ pC/N at the sintering temperature of ~ 1090 °C. For k_p value, a similar variation trend was observed in $\text{KN}_{0.56}\text{N-BNZ-BF}$ ceramics. In addition, the Q_m value (~ 50) keeps stable in all range of sintering temperature. Figure 10b shows the relationship of d_{33} and relative density of $\text{KN}_{0.56}\text{N-BNZ-BF}$ ceramics as a function of sintering temperature. We can see that d_{33} and relative density of $\text{KN}_{0.56}\text{N-BNZ-BF}$ ceramics first increases and then drops with increasing the sintering temperature, getting a higher d_{33} and preferably density at the sintering temperature of ~ 1090 °C. Therefore, the sintering temperature can seriously influence the density of the ceramics, and then effect on the piezoelectric properties.

Figure 11 plots the thermal stability of d_{33} of $\text{KN}_{0.56}\text{N-BNZ-BF}$ ceramics. One can see that the normalization d_{33} decreased slightly with increasing the annealing temperature (T_a) to 300 °C, and remain more than 88.1% when the T_a is less than 300 °C. Continuing increasing the T_a to the T_c of this ceramics, it decreases dramatically. Therefore, the ceramics with $x = 0.56$ demonstrate a good thermal stability of d_{33} at $T_a \leq 300$ °C, which is very useful for practical applications.

4 Conclusion

In this work, $\text{KN}_x\text{N-BNZ-BF}$ lead-free ceramics were fabricated by conventional ceramic technique. The K/Na ratio strongly affects the microstructure, phase structure and electrical properties of $\text{KN}_x\text{N-BNZ-BF}$ ceramics. With increasing the Na content, a series of phase transitions from R–O–T (~ 0.44 – 0.60) to O–T (~ 0.64 – 0.68) was observed in the ceramics. By tailoring their K/Na ratio and optimizing the sintering temperature, an enhanced electrical properties (e.g. $d_{33} \sim 438$ pC/N, $k_p \sim 0.51$, $T_c \sim 320$ °C, $\varepsilon_r \sim 2304$ and $\tan \delta \sim 0.029$) was obtained at the ceramics with $x = 0.56$ sintered at 1090 °C, which could be attributed to the preferably density as well as the R–O–T phase boundary nearer the room temperature. In addition, a good thermal stability of d_{33} ($T_a \leq 300$ °C, Normalization $d_{33} \geq 88.1\%$) was obtained in the ceramics with $x = 0.56$. Therefore, we think that the $\text{KN}_x\text{N-BNZ-BF}$ ceramic is a promising candidate for piezoelectric devices.

Acknowledgements This work was supported by Project (Grant Nos. KYTZ201312 and J201220) Supported by the Scientific Research Foundation of CUIT, the Fundamental Research Funds for the Central Universities of Southwest University for Nationalities (No. 2014NZYQN11), the Foundation of Sichuan province science and technology support program, China (Grant No. GZ0198) and Scientific Research Project of Sichuan Provincial Department of Education (Grant No. 16ZA0216).

References

1. S. Zhang, R. Xia, T.R. Shrout, J. Electroceram. **19**, 251 (2007)
2. B. Jaffe, W.R. Cook, H. Jaffe, *Piezoelectric Ceramics* (Academic Press, New York, 1971)
3. EU-Directive 2002/96/EC, Waste electrical and electronic equipment (WEEE). Off. J. Eur. Union **46**(L37), 24 (2003)
4. EU-Directive 2002/95/EC, Restriction of the use of certain hazardous substances in electrical and electronic equipment (RoHS). Off. J. Eur. Union **46**(L37), 19 (2003)
5. B. Wu, C. Han, D.Q. Xiao, Z. Wang, J.G. Zhu, J.G. Wu, Mater. Res. Bull. **47**(11), 3937 (2012)
6. B. Wu, D.Q. Xiao, W.J. Wu, J.G. Zhu, Q. Cheng, J.G. Wu, Ceram. Int. **38**(7), 5677 (2012)
7. Y. Saito, H. Takao, T. Tani, T. Nonoyama, K. Takatori, T. Homma, T. Nagaya, M. Nakamura, Nature **432**, 84 (2004)

8. B. Wu, D.Q. Xiao, J.G. Wu, Q. Gou, J.G. Zhu, *J. Mater. Sci.: Mater. Electron.* **26**(4), 2323 (2015)
9. R.Z. Zuo, C. Ye, X.S. Fang, *J. Phys. Chem. Solids* **69**, 230 (2008)
10. B. Wu, D.Q. Xiao, J.G. Wu, Q. Gou, D.D. Mazhao, J.G. Zhu, *Ferroelectrics* **489**(1), 129 (2015)
11. B. Wu, J.G. Wu, D.Q. Xiao, J.G. Zhu, *Dalton Trans.* **44**(48), 21141 (2015)
12. J. Wu, D. Xiao, J. Zhu, *Chem. Rev.* **115**(7), 2559 (2015)
13. T. Takenaka, H. Nagata, *J. Eur. Ceram. Soc.* **25**(12), 2693 (2005)
14. F.Z. Yao, K. Wang, W. Jo, J.F. Li, *Adv. Funct. Mater.* **26**, 1217 (2016)
15. W.F. Liang, W.J. Wu, D.Q. Xiao, J.G. Zhu, *J. Am. Ceram. Soc.* **94**(12), 4317 (2011)
16. N. Liu, K. Wang, J.F. Li, Z. Liu, *J. Am. Ceram. Soc.* **92**(8), 1884 (2009)
17. J.G. Wu, D.Q. Xiao, Y.Y. Wang, J.G. Zhu, L. Wu, Y.H. Jiang, *Appl. Phys. Lett.* **91**(25), 252907 (2007)
18. D. Damjanovic, N. Klein, J. Li, V. Porokhonsky, *Funct. Mater. Lett.* **3**, 5 (2010)
19. X.P. Wang, J.G. Wu, D.Q. Xiao, J.G. Zhu, X.J. Cheng, T. Zheng, B.Y. Zhang, X.J. Lou, X.J. Wang, *J. Am. Chem. Soc.* **136**, 2905 (2014)
20. K. Xu, J. Li, X. Lv, J.G. Wu, X.X. Zhang, D.Q. Xiao, J.G. Zhu, *Adv. Mater.* **28**, 8519 (2016)
21. L. Fu, D. Lin, Q. Zheng, X. Wu, C. Xu, *Phys. Status Solidi (a)* **209**(11), 2299 (2012)
22. D. Lin, K.W. Kwok, H.L.W. Chan, *J. Appl. Phys.* **91**, 167 (2008)
23. J.G. Wu, D.Q. Xiao, Y.Y. Wang, J.G. Zhu, P. Yu, *J. Appl. Phys.* **103**, 024102 (2008)
24. L. Wu, J.L. Zhang, C.L. Wang, J.C. Li, *J. Appl. Phys.* **103**, 084116 (2008)
25. Y.J. Dai, X.W. Zhang, K.P. Chen, *Appl. Phys. Lett.* **94**, 042905 (2009)
26. J.G. Wu, D.Q. Xiao, Y.Y. Wang, J.G. Zhu, L. Wu, *Appl. Phys. Lett.* **91**, 252907 (2007)
27. L. Wu, J.L. Zhang, S.F. Shao, P. Zheng, C.L. Wang, *Appl. Phys. Lett.* **41**, 035402 (2008)
28. V.J. Tennery, K.W. Hang, *J. Appl. Phys.* **39**, 4749 (1968)
29. M. Ahtee, A.M. Glazer, *Acta Crystallogr.* **32**, 434 (1976)
30. B.Y. Zhang, J.G. Wu, B. Wu, J.G. Wu, D.Q. Xiao, J.G. Zhu, *J. Alloys Compd.* **525**, 53 (2012)
31. J.G. Wu, X.P. Wang, X.T. Zheng, B.Y. Zhang, D.Q. Xiao, J.G. Zhu, X.J. Lou, *J. Appl. Phys.* **115**(11), 114104 (2014)
32. S.S. Feng, D.Q. Xiao, J.G. Wu, F.X. Li, M. Xiao, J.G. Zhu, *J. Electroceram.* **34**(2–3), 142 (2015)
33. B.P. Zhang, J.F. Li, K. Wang, *J. Am. Ceram. Soc.* **89**, 1605 (2006)
34. E. Rigaard, T. Wurlitzer, *J. Eur. Ceram. Soc.* **25**, 2701 (2005)
35. J.F. Tressler, S. Alkoy, R.E. Newnham, *J. Electroceram.* **2**(4), 257 (1998)